ISSN: 0975-833X

Available online at http://www.journalcra.com

International Journal of Current Research
Vol. 9, Issue, 08, pp.55614-55619, August, 2017

INTERNATIONAL JOURNAL OF CURRENT RESEARCH

RESEARCH ARTICLE

PROFICIENT MODELLING TECHNIQUES TO ACHIEVE NANO PHOTONICS

*Manush Nandan, M. and Narendiran

ECE Department, RMD Engineering College, Kavaraipettai, Chennai, Tamilnadu, India

ARTICLE INFO

Article History:
Received 20th May, 2017
Received in revised form
23rd June, 2017
Accepted 09th July, 2017
Published online 31st August, 2017

Key words:

Nano photonics, Waveguide, Gap soliton, Polarisation, Photonic crystal, Core, Cladding.

ABSTRACT

Hemangiomas can occur anywhere in body tissue which having vascular component including skin, mucosa, muscles, glands, viscera and bones. Intramuscular hemangiomas (IMH) of the head and neck are uncommon benign vascular tumors as compare to cutaneous hemangioma, for which head and neck region is the most common location (60%). Head and neck IMH arises frequently in the masseter and trapezius muscle. However, hemangiomas of the retropharyngeal space are extremely rare in literature, with only few cases reported till date and for such cases, magnetic resonance imaging (MRI) is found significant diagnostic tool over other imaging studies.

Citation: Manush Nandan, M. and Narendiran, 2017. "Proficient modelling techniques to achieve nano photonics", *International Journal of Current Research*, 9, (08), 55614-55619.

INTRODUCTION

The volume of digital data conveyed around the globe rises briskly every single year. Whenever large amount of data has to be transferred, or whenever the data needs to be transmitted across greater surface area, optical fibers are the ideal medium for mobility, due to their low losses, and high capacity. A single optical fiber (whose core is less than 10μm in diameter) has been verified to transmit more than 1Tbit/sec, with losses less than 0.2dB/km. By the same sign, this large amount of data needs to be processed. To perform nearly any kind of process on optical signals today (like pulse regeneration, wavelength conversion, bit-rate conversion, logic operation, etc.) the signals first need to be converted to the electronic field. Unluckily, there are vital physical explanations that hinder the field of electronics from operating well at high frequencies. As a result, the price of electronic components grows rapidly when more sophisticated bit-rates are required, and hence, use all optical signal processing becomes briskly more and more pre dominant. Since the signal processing needs to be done on rapid-fast pace, the only mechanism at discarding is to explore a material's optical non-linearities. Most researches today is in the area of optical devices which is in high-index-contrast integrated optics. Regrettably, these devices suffer from major losses due to unevenness at the faces of their waveguides, and are highly polarization sensitive.

****Corresponding author:*** **Manush Nandan, M.**
ECE Department, RMD Engineering College, Kavaraipettai, Chennai, TamilNadu, India.

Another approach involves the use of in-fiber all-optical devices, which would prevent these drawbacks. But, silica fiber non-linearities are very low, which combined with their large modal area results into signals having to be disseminated for very long distances before the non-linear effects become evident. Many exciting switching schemes involving excitation of gap solitons can reduce the power necessities, but need a episodic grating along the axial direction, which rises the execution desires. In this work we show how the use of photonic crystals can provide a solution for many of these drawbacks. Photonic crystals (Joannopoulos *et al.,* 1995; Photonic Crystals and Light Localization, 2000) are said to be periodic dielectric arrangements that provide a peculiar control over the flow of light within them. The primary significance is the presence of a band gap of photonics, a frequency range for which light propagation is distributed in all directions. In that sense, the photonic crystal's control over the flow of light can be seen as the equivalent of photonics to the semiconductor's control over the flow of electrons. Impurity levels that trap light at frequencies within the band gap can be modelled inside the photonic crystal in terms of appropriate structural defects, leading to extremely high Q cavity modes. In the way, linear arrays of defects inside a photonic crystal may lead to guided modes within the band gap, leading to waveguides without any radiation losses. First, we must overcome the problem of radiation losses and polarization-sensitivity of integrated optical systems. Beginning with a platform of 3D photonic crystal integration, we can design waveguides by means of introducing linear defects into the photonic crystal, in such a way that a guided defect-mode appears within the photonic band gap. It is known that in these waveguides radiation losses can be completely removed, even at features such as sharp bends, while achieving resonant 100% transmission for a wide range of frequencies. However, the photonic crystals, and any waveguides produced within them, are highly-polarization selective. It may then seem counter-intuitive that such a system could ever be tuned to provide a polarization-insensitive response. We show that with the correct selection of a 3D photonic crystal, and the utilization of the structure symmetries and the extreme control on the flow of light provided by the photonic crystal, it is possible to do just that. We create doubly-degenerate polarization-insensitive waveguides, that can bend light around sharp corners with high efficiency and zero radiation losses. Next, we address the problem of in-fiber switching. Recently, a new type of fiber (a photonic band gap fiber called Omni Guide fiber) has been proposed. Materials used in this fiber are chalcogenide glasses which typically have Kerr coefficients 100-1000 times higher than that of silica.

In addition, since this is found to be a high-index contrast fiber, modal ranges can be 1000-100 times smaller. Consequently, the non-linear response of these fibers is orders of magnitude larger than in silica fibers, making them an ideal non-linear medium. We show that nonlinear gap solitons can exist in such fibers. Gap solitons are nonlinear excitations in a medium within which linear (low intensity) propagation is not allowed, and are created by the balance between the strong fiber dispersion and the material nonlinearity. They can be used to implement many all-optical operations (Fink *et al.,* 1999) including all-optical logic, pulse regeneration and reshaping, creation of ultra narrow pulses starting from continuous wavelength (CW) signals, etc. Up until now, gap solitons have been exclusively studied in periodically modulated systems, which provide the extremely strong dispersion for frequencies satisfying the Bragg condition, i.e. for frequencies within the band gap.

Here we find that because of the unique dispersion relation of the guided modes in photonic band gap fibers, which involves a frequency cut-off at k=0, we do not need the axial periodicity in order to excite gap solitons. Bistability and optical swiching are thus demonstrated for the first time in an axially uniform system. Such systems have small power and implementation requirements, and may be ideal for all optical in-fiber devices. We use the finite-difference time-domain (FDTD) method (Johnson *et al.,* 2011) to simulate the propagation of electromagnetic pulses through the photonic crystal structures. We solve the exact full-vector time-dependent Maxwell's equations on a computational grid:

$$\nabla \times \vec{E} = -\mu \frac{\partial \overrightarrow{H}}{\partial t} \; ; \; \nabla \times \vec{H} = \frac{\partial \overrightarrow{D}}{\partial t} \quad \ldots\ldots\ldots\ldots\ldots\ldots\ldots\ldots\ldots\ldots \text{(1)}$$

For simulating unbounded systems (radiation boundary conditions) we use perfectly-matched-layer (PML) boundary conditions at the edges of the simulation cells.

Modelling of nano photonics

Modelling of nano-photonics is obtained by polarization – independent waveguides or by gap soliton formation and optical switching. Based on the requirement the suitable modelling can be chosen for the modelling of nano-photonics.

A. Polarization-independent waveguides

Lossless guiding of light at length-scales approaching the wavelength of the light itself is a necessary property for any future integrated optical circuit. While high index-contrast dielectric waveguides can reduce radiation losses from features such as sharp bends, they cannot completely suppress them and are in general very sensitive to roughness. Photonic crystals (Joannopoulos *et al.,* 1995; Photonic Crystals and Light Localization, 2000), on the other hand, have been shown in certain cases to eliminate radiation loss (Analui *et al.,* 2006; Soljacic *et al.,* 2002) and thus offer a promising platform for designing high-performance waveguide networks. A common drawback, however, to all high-index and photonic-crystal waveguide systems proposed to-date (2D or 3D systems), remains that they are highly polarization selective. Given that the polarization-state of an input signal may not be known and/or may vary over time, their proper operation would require the use of active polarization pre-processing devices. In this work, we demonstrate that by utilizing the symmetries of a proper choice of 3D photonic crystal, one can tune line defects to create guided modes inside the spectral gap that are essentially degenerate, with a polarization-insensitive dispersion relation.

We further demonstrate the stability of these modes to symmetry breaking by simulating high-transmission polarization- independent light guiding around a sharp bend. This is the first structure exhibiting such polarization-insensitive transmission at such length scales. One approach to polarization insensitivity would be to design a photonic crystal with line defects possessing the appropriate cross-sectional symmetry for polarization degeneracy. Another approach is to employ a photonic crystal consisting of two kinds of photonic crystal slabs, each best suited for confining one of two possible polarizations. The latter approach results in planar arrays of defects, which are amenable to micro-fabrication, and is the method used here. The photonic crystal provides precisely this capability, consisting of alternating slabs of dielectric rods in air (*rod* layers, appropriate for confining TM-polarized waves) and air holes in dielectric (*hole* layers, appropriate for confining TE-polarized waves). Wave-guiding structures can be designed within this crystal by introducing planar line defects in the *hole* and/or *rod* layers, resulting in the formation of defect (guided) bands inside the band gap. A remarkable property of this 3D crystal is that the resulting guided modes are very similar to the 2D TE- and TM-polarized modes one gets from solving a 2D problem with the dielectric constant defined by the corresponding cross section along the defect plane. Hence, in the 3D crystal, a sequence of larger holes in a *hole* layer results in a TE-like mode pulled up from the dielectric band, predominantly polarized with its magnetic field normal to the defect plane. Similarly, a sequence of smaller rods in a *rod* layer also results in a TM-like mode pulled up from the dielectric band, but now predominantly polarized with its electric field normal to the defect plane. Note that these modes are approximately even (TE) and odd (TM) under reflection on a plane parallel to the *hole* and *rod* layers. In a purely 2D system this symmetry is exact, prohibiting mode mixing even at lattice distortions such us bends or disorder. This is a key criterion needed to induce a significant suppression of mode mixing at similar planar lattice distortions. Due to the omnidirectional gap provided by the photonic crystal, the above procedure enables the design of wavelength-scale minimal-loss waveguide networks for both polarizations. While this is promising for integrated optical systems, still, it does not overcome one of integrated optics' old problems: each polarization satisfies a different dispersion relation, resulting in different propagation properties such as speed and pulse broadening, thus leading to a different response in any device. However, if we combine the two sequences of line defects in a way so that the two guided modes are close spatially yet maintain different symmetry, we may tailor the defect structures to enforce an "accidental degeneracy" in the guided dispersion relations, i.e. to have them coincide. In this regard, it is important to identify a symmetry operation along the guide direction, with respect to which the two modes (eigenstates) transform oppositely, so that a tailored defect structure respecting this symmetry will not result in mode mixing and repulsion.

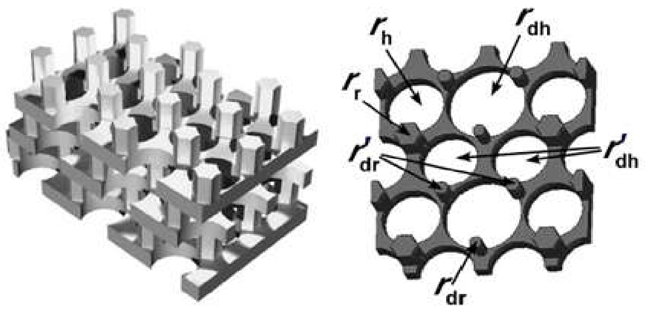

Fig. 1. The photonic crystal used in our simulations (left). A schematic of a small segment of the waveguide (right). Only the two layers of the 3D crystal involving the planar line defects are shown for clarity

A portion of our structure consisting of two layers is shown in Fig. 1. We create our waveguides along the set of {[211]} (second nearest neighbour) directions, because there is a mirror plane perpendicular to the layers, lying along the axis of a straight {[211]} waveguide, for both the *hole*- and *rod*-layer line defects. This distinguishes the TE-like and TM-like modes into different irreducible representations. In contrast, had we chosen a waveguide along the {[011]}(nearest neighbor) directions, the only symmetry operation that leaves both the *hole*- and *rod*-layer line defects invariant is a 180^o rotation along {[011]}. However, this operation cannot distinguish between TE-like and TM-like modes. The detailed structure of the photonic crystal is reported. The hole radius within the *hole* layer is r_h=0.414a and the equivalent-rod[23]radius within the *rod* layer is r_r=0.175a, where a is the in-plane lattice constant and is related to the fcc lattice constant a_{fcc} by a=a_{fcc} / 2. We use a dielectric contrast of 12, for which a band gap of 21% is obtained.

The first step is to introduce two line-defects to create two guided modes of opposite polarization: larger holes (r_{dh}=0.53a) in the *hole* layer (which will support the TE-like odd mode) and smaller rods (r_{dr}=0.08a) in the *rod* layer (which will support the TM-like even mode). The dispersion relations of these two modes, calculated by the FDTD method, are shown in Fig. 1a. They differ in both their center frequency and their bandwidth. A key property, however, is that they are both well described by a cosine dispersion relation, which makes them easier to match. This cosine dispersion relation arises because our waveguides are very similar to a chain of weakly coupled defects. For stronger coupling, it is expected that the dispersion relations will divert from the simple cosine form and it will thus become progressively difficult to match them. We will use these two bands as a starting point and perturb the surrounding crystal elements to force accidental degeneracy.

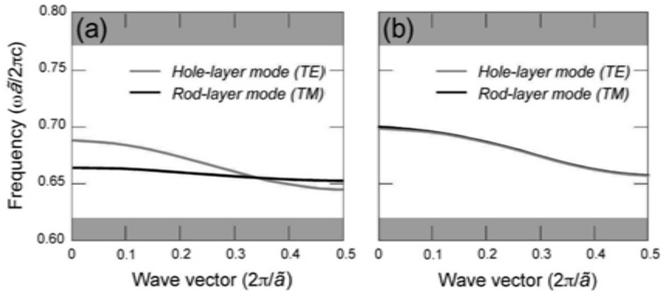

Fig. 2. Dispersion relations for the guided modes resulting from planar line defects in the 3D photonic crystal, (a) before and (b) after the tuning

Gray areas mark transmission bands while white areas mark band gaps. Changes in the dielectric elements around the waveguide can be effectively though as the addition or removal of dielectric material from the high field-intensity regions. These changes will introduce a frequency shift in the corresponding dispersion relations. This shift is maximal for changes in regions of high field intensity, and minimal for changes in regions of low field intensity. Also, the frequency shift is positive when remove dielectric material and negative when we add dielectric material. A pulse with a Gaussian profile in time is launched at the entrance of the waveguide, and the fields are monitored at two positions, as shown in Fig. 3. Position A is located halfway between the source and the bend and is the observation point for the incident and reflected pulses, while position B is located 12$\tilde{a}$ after the bend and is the observation point for the transmitted pulse. Minimal secondary reflections at the edges of the computational cell are still present, but they appear at later times and do not contaminate the useful data. We find that most of the energy is transmitted through the bend. As expected, the symmetry breaking at the bend results in transmitted and reflected pulses that are composed of both modes. However, this mixing is very small, comparable to half the overall reflection from the bend (see Fig. 3).

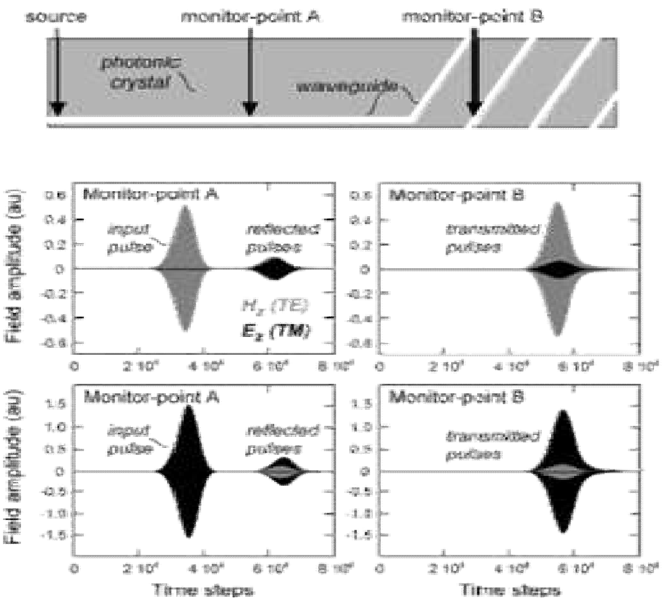

Fig. 3. Top panel: Schematic of the simulation system for studying transmission through a bend

The waveguide, defined by the white line, "wraps around" after the bend using periodic boundary conditions, minimizing the required computational cell. Monitor points are at A and B. Bottom panels: Simulation results. Fields at the observation points A and B, which are located before and after the bend respectively. Each polarization is studied separately with points A and B centered in the appropriate layer in each case. Gray is used for the H_z field of the TE-like mode and black for the E_z field of the TM-like mode. A pure TE(TM)-like mode will have zero $E_z(H_z)$ field at its symmetric center, as is the case for the incident pulses. In order to quantify the transmission through the bend, we study the frequency-resolved pulses going in and out of the bend. Since these are not single-mode waveguides, we must use data from flux-monitoring planes, positioned at A and B. For better resolution, as well as a consistency test, we use two pulses of different center frequencies per polarization, as shown in the top panels of Fig. 4. The corresponding ratios of the fluxes at A and B provide the transmission and reflection coefficients, as shown in the bottom panel of Fig. 4. These coefficients add up to 1 for all frequencies, with an error of less than 1%. We find a wide frequency range of high transmission for both modes, and a frequency $t\tilde{a}/2/c=0.6835$ for which the transmissions coincide to 94.5%. Note that, as expected, resonant transmission is observed at different frequencies for the two modes: at lower frequencies for the TE-like mode and higher frequencies for the TM-like mode. Also note that the TM mode does not actually achieve 100% transmission at any frequency within the useful bandwidth.

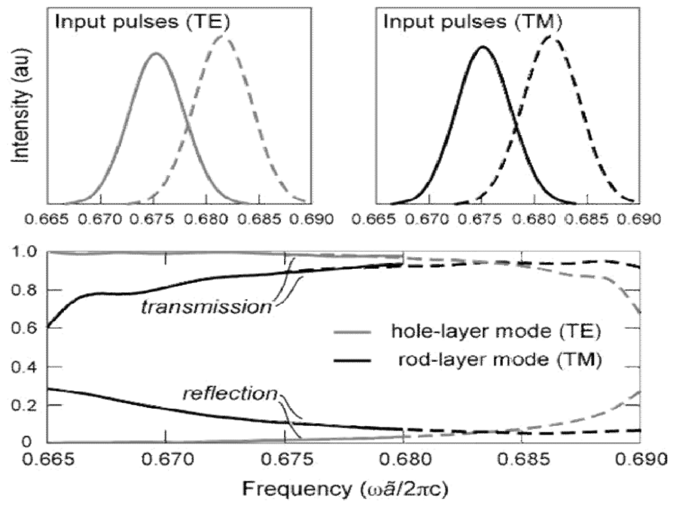

Fig 4. Top panels: Spectral profile of the input pulses used in the numerical experiments for the TE-like and the TM-like modes

Bottom panel: By taking appropriate ratios of transmitted, reflected and input pulses we extract the corresponding transmission and reflection coefficients. Around the common transmission frequency, we resolve the calculated fluxes into the two modes, in order to quantify the degree of modal mixing. We find that mixing is generally small, and that it monotonously decreases for increasing frequency (from about 5% at $t\tilde{a}/2/c=0.675$ to less than 1% at $t\tilde{a}/2/c=0.69$). At the common high-transmission frequency, the transmitted power retains its polarization to about 97%. The absence of strong modal mixing is due to the approximate horizontal mirror plane symmetry, as was mentioned earlier. The TE-like and TM-like modes appear as two different representations of a single horizontal symmetry plane, thus resulting in minimal mode mixing in the bend region. An important point to note here is that the field pattern of the two modes is different. This will manifest into different coupling coefficients with a symmetric input such as from a fiber. It will thus be necessary to tailor the input part of the waveguides in order to match the coupling coefficients, and thus achieve polarization-insensitive excitation. This however, goes beyond the scope of this paper.

B.Gap solitons in axially uniform fibers

Gap solitons and optical switching have been extensively studied in nonlinear dielectric structures with a one-dimensional axial periodicity in their linear refractive properties. Corresponding experimental realizations include waveguide24 or fiber Bragg gratings and integrated multi-layer hetero structures. Such periodic systems exhibit spectral gaps of high reflectivity for wave-propagation along the axial direction. For intense light illumination at a frequency inside one of the gaps and with an optical nonlinearity present, these systems can exhibit solutions whose envelopes take the form of solitary waves. Such solutions, called gap-solitons or Bragg-solitons, introduce a strong power-dependence to the transmissivity, at some powers achieving even full resonant transmission. In some cases a bistable response may be observed, i.e. one of two different transmissivities are possible at the same input power, making the actual optical response a function of the system's history. Such periodic structures are very attractive for all-optical switching, logic-gate operation, memory etc. Because of the necessity of a spectral gap for their existence, gap solitons and gap-soliton-mediated bistability have been exclusively studied in systems with axial periodicity. In this work, we show that gap-soliton excitation is also possible in axially-uniform photonic bandgap (PBG) fibers. These fibers are laterally grated forming a PBG cladding that surrounds the core. Guiding is achieved through a cladding gap-condition, in contrast to usual fibers where guiding is achieved through total internal reflection. We show that in the presence of an optical Kerr-type nonlinearity, such axially-uniform PBG fibers exhibit gap-soliton generation and gap-soliton-mediated bistability. The observed nonlinear response is a direct consequence of the particular guided-mode dispersion relation, which involves a frequency cut-off at k=0, and is unique among axially uniform systems to high index-contrast PBG fibers, and metallic waveguides.

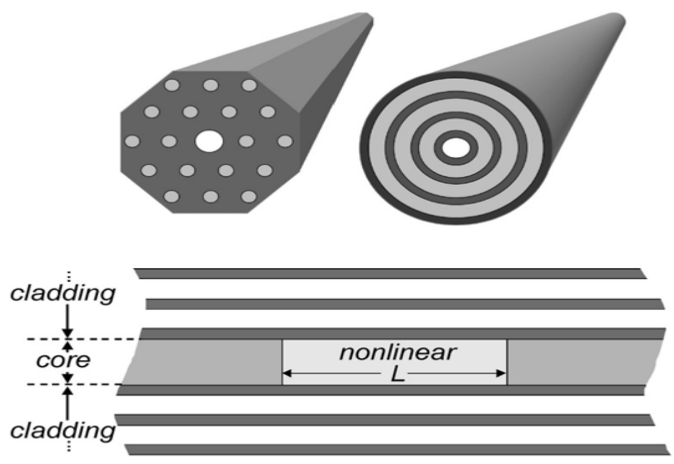

Fig. 5. Top: Schematics of two photonic band gap fibers, the Holey fiber and the Omni guide fiber respectively. Bottom: The 2D simulation system which is an embodiment of the Omni guide fiber

Cladding consists of alternating dielectric layers of high-index (2.8) with thickness 0.3a and low-index (1.5) with thickness 0.7a, where a is the period of the cladding layers and serves as the unit of length. The core has a diameter d linear=d nonlinear = 1.2a and consists of linear material (darker gray) with index n=1.9 and nonlinear material (lighter gray) with index $n\varpi$= n0+n2|E|2, where n0=1.6. The guiding direction is parallel to the layers. We study a two-dimensional embodiment of PBG fibers, described fully in Fig. 5. This system captures the most essential features of the 3D fiber, in particular, guided-mode dispersion relations with a frequency cut-off at k=0, and the absence of a full spectral gap. For example in Fig. 7a we superimpose the dispersion relations for the linear material and for the nonlinear material when $n\varpi$=n0=1.6, as calculated by the FDTD method. In each case there is a frequency cut-off at k=0 which we denote as τc for the linear material and $\sigma\chi$ for the nonlinear material. The difference in refractive index results in an almost parallel shift in dispersion relations. Any other choice of refractive indexes and structural parameters should suffice as long as one has single mode operation and $\tau\varpi c > \tau c$. For example, setting n=n0∗1 and shrinking the nonlinear core d nonlinear<d linear would have a similar effect, since guided modes with a reduced modal area appear at a higher frequency, and thus with an increased cut-off frequency. This is particularly important in terms of implementation and applications, since there exist many easy ways for externally controlling the dispersion relation, such as mechanical strain, temperature, radiation, etc.

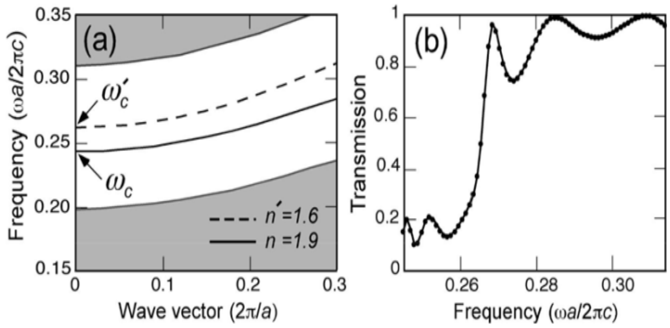

Fig. 6. (a) Dispersion relations calculated by the FDTD method for two values of the core index. . (b) Transmission coefficient vs frequency for a linear-material system with an $n\varpi$=n0=1.6 defect core of size L=5a

The cut-off frequencies are τc = 0.244 and $\tau\varpi c$ = 0.26215. Gray areas represent cladding and radiation modes, where light is either guided through the cladding or escapes out of the fiber. These modes cover the entire frequency region at higher wave vectors. At low input power, guided waves in the linear-material core (i.e. $\tau > \tau c$) should be strongly reflected upon incidence on the nonlinear region if $\tau < \tau c\varpi$. Such a linear transmission coefficient is shown in Fig 6b. At high input power, however, we should observe a wide range of nonlinear phenomena, similar to those found in the study of nonlinear periodic gratings. For example, a power-dependent frequency shift of the nonlinear-material's dispersion relation should result into a power-dependent transmission, such as in optical limiting systems. For the proper sign of n2 (n2>0 in our case), we should also observe the excitation of resonant structures such as gap solitons, resulting in resonant transmission and bistability. It is the latter effects in the limit of small nonlinearities (which is the experimentally correct limit anyway) that will be our focus here. In Fig 7 we plot the intensity along the nonlinear core as a function of time, around the switch-up point for the L=5a system (CW response). It can be seen how the gap soliton is excited in the structure. At first it undergoes a damped oscillation until it reaches equilibrium. These oscillations are well correlated with the fluctuations of the output in Fig 8b. This transient time is a measure of the response (switching) time of our device, which is of the order of 200 periods (for η=1.55mm this time is about 1ps). A similar plot (not shown), but inverted and with less fluctuations is obtained at the switch-down point. In the L=8a case, on the other hand, these oscillations are not damped, and so the soliton does not reach equilibrium, but rather it gets transmitted out of the nonlinear core, only to be followed by a new soliton, resulting into a periodic train of pulses in the output. The peak intensity of each pulse is about 10 times larger than that of an equivalent transmitted CW. The duration of each pulse is about 20 periods and the pulses appear at a frequency of about 100 periods (for η=1.55 $\propto$m this is a pulse width of about 100 fs at a period of about 500 fs). In Fig 9 we plot the intensity along the nonlinear core for the L=5a system at two different points: at the peak of the upper transmission branch where a gap soliton has been excited (at time5900T of Fig 7), and at the lower branch where the wave decays exponentially (at time5400T of Fig 7).

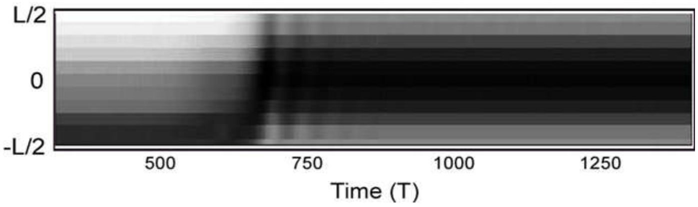

Fig. 7. Intensity along the nonlinear core as a function of time, around the switch-up point for the L=5a system (CW response)

Darker regions mark higher intensity. The vertical axis is the axial (propagation) direction, with the input is at –L/2 and the output at L/2. Before the switch-up, the intensity decays along the axial direction, while after switch-up, the intensity is maximum in the center of the nonlinear core, corresponding to a gap soliton.

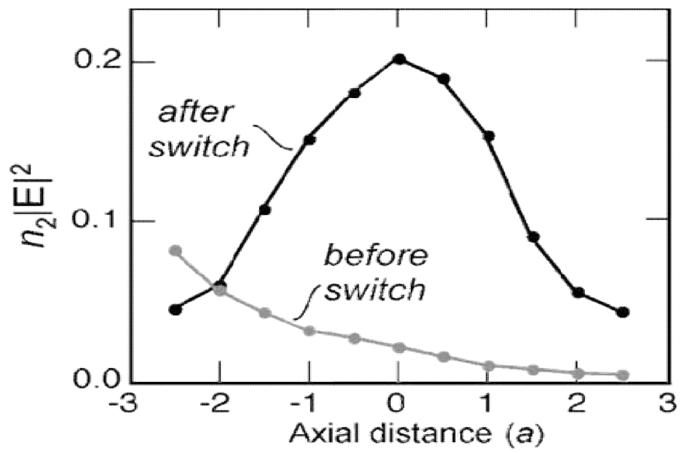

Fig. 8. Normalized intensity (or local index change βn=n2|E|2) along the nonlinear core for the L=5a system at, the peak (100% resonant transmission) of the upper transmission branch (black), and, at the lower transmission branch (gray)

The excitation of a gap soliton is seen at the resonant transmission case. Our axially uniform nonlinear system responds very similarly to a nonlinear Bragg grating system. However, it is different in terms of performance and implementation. Having no need for a periodic modulation it is easier to make. Materials used in these fibers are chalcogenide glasses which are highly nonlinear, and so all that is needed is a frequency cut-off. This can be achieved by replacing part of the core with a lower index nonlinear material (as we did here), or alternatively, it can be achieved by external means, such as mechanical strain, temperature, radiation, etc. For example, shrinking part of the core by externally creating a constriction will have the same effect in creating a frequency cut-off. Given that the device's mode of operation (CW or pulsed) depends on the device structural parameters, we can use these external means to control its operation, without having to change the input power or frequency.

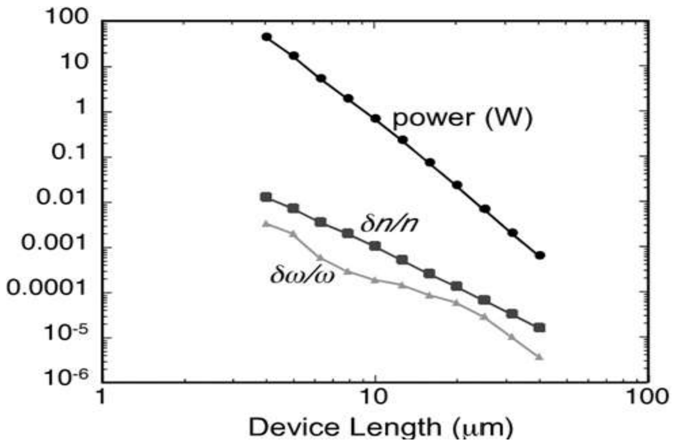

Fig. 9. Power and bandwidth requirements for the proposed device as a function of its nonlinear core size

For chosen parameters η=1.55 μm and n2=1.5×10-13 cm2/W. Power is measured at the switch-up point at which the width of the bistable loop is 10% of its mid-input power. Bandwidth βτ/τ is the frequency change necessary to change the switch-up power by 10%.Finally, we used a simplified 1D nonlinear model based on a fit of the dispersion relations of Fig 7a, to estimate how various experimental parameters would depend on the system's size L. We do not present details of this model here. We have found the 1D model's predictions to agree well with the simulation data and it is thus a valid and useful tool for practical estimates. We calculated the operating power P, the maximum nonlinear index change induced βn/n and the operational bandwidth βτ/τ as a function of L, while we tuned the frequency so that the width of the bistable loop is 10% of its center intensity. These results are shown in Fig 9. We find that all three quantities drop exponentially with increasing size L. As a quantitative example, a system with an nonlinear core length of L=10∝m operating at a vacuum wavelength of η=1.55∝m (i.e. a=0.406∝m) and with a nonlinear coefficient of n2 = 1.5 υ10<13 cm 2 / W (typical of many chalcogenide glasses), requires an operating power of about P=800mW, a maximum nonlinear-index-change of about βn/n=0.001, and offers a bandwidth of about βτ/τ=0.0002540GHz.

Conclusion

Thus, the various photonics techniques used for communication, selecting model of nano photonics are explained. In conclusion, we have shown only one case where the use of photonic crystals can lead to novel and improved designs of optical nano components and nano devices in photonics. a) We have shown that polarization-independent waveguides and waveguide bends can be designed in a particular class of 3D photonic crystals by means of forced accidental degeneracy. The only requirement is the existence of two well-localized modes of definite and opposite symmetry. Further improvements and/or creation of novel polarization-processing devices should be possible by optimizing the structure parameters. b) We have studied an axially uniform nonlinear system that exhibits gap-soliton formation and optical switching. This ability to obtain soliton formation and switching without imposing axial periodicity may lead to new design and fabrication opportunities for eventual experimental realization of all-optical nano devices. Also now the future research will be more focused on the safety, security and efficiency. The security must be of top notch level to prevent hacking or any unauthenticated use.

REFERENCES

"Silicon Integrated Nanophotonics". IBM Research. Retrieved 14 July 2009.

Almeida, V.R., Barrios C.A., Panepucci R.R., Lipson, M. 2004. "All-optical control of light on a silicon chip". *Nature*, 431(7012):10811084.Bibcode:2004Natur.431.1081A.doi:10.1038/nature02921. PMID 15510144.

Analui, B. *et al*., A fully integrated 20-Gb/s optoelectronic transceiver implemented in a standard 0.13-um CMOS SOI Technology, *IEEE J. Solid State Circuits*, 41 (12), p. 2945,2006.

Fink, Y., D.J. Ripin, S. Fan, C. Chen, J.D. Joannopoulos, and E.L. Thomas, 1999. *J. Lightwave Tech.,* 17, 2039.

Guiding, Modulating, and Emitting Light on Silicon–Challenges and Opportunities". *Journal of Lightwave Technology*, 23(12):42224238. Bibcode: 2005JLwT...23. 4222L. doi:10.1109/JLT.2005.858225.

Jalali, Bahram; Fathpour, Sasan, 2006. "Silicon photonics". *Journal of Lightwave Technology,* 24 (12): 46004615. Bibcode:2006JLwT...24.4600J.doi:10.1109/JLT.2006.8857 82.

Joannopoulos, J.D., R.D. Meade, and J.N. Winn, 1995. Photonic Crystals (Princeton, New York).

Johnson, S.G., M. Ibanescu, M. Skorobogatiy, O. Weisberg, T.D. Engeness, M. Soljacic, S.A. Jacobs, J.D. Joannopoulos, and Y. Fink, 2001. Optics Express 9, 748.

Narasimha, A. *et al*. 2008. A 40-Gb/s QSFP optoelectronic transceiver in a 0.13 mm CMOS SOI technology Opt. Fiber Comm. Conf. (OFC), February.

Photonic Crystals and Light Localization, edited by C.M. Soukoulis, Proceedings of the NATO ASI on Photonic Band Gap Materials, Limin Hersonissou, Crete, Greece, 19-30 June 2000 (Kluwer Academic, Dordrecht, 2001).

Soljacic, M., M. Ibanescu, S.G. Johnson, J.D. Joannopoulos, and Y. Fink, 2003. *Opt.Lett*. 28, 516.

Soljacic, M., M. Ibanescu, S.G. Johnson, Y. Fink, and J.D. Joannopoulos, 2002. *Phys. Rev.,* E 66, 055601R.

Temelkuran, B., S.D. Hart, G. Benoit, J.D. Joannopoulos, and Y. Fink, 2002. *Nature,* 420, 650.

Winful, H.G., J.H. Marburger, and E. Garmire, 1979. Appl. Phys. *Lett*., 35, 379.

Witzens, J. *et al*., 2008. 10Gbit/s transceiver on silicon Proc.SPIE6996, April, doi:10.1117/12.786641

****